UCRL-17212

University of California

Ernest O. Lawrence Radiation Laboratory

DEFORMATION AND FRACTURE OF GOLD-PLATINUM POLYCRYSTALS STRENGTHENED BY SPINODAL DECOMPOSITION

TWO-WEEK LOAN COPY

This is a Library Circulating Copy which may be borrowed for two weeks. For a personal retention copy, call Tech. Info. Division, Ext. 5545

Berkeley, California

DISCLAIMER

This document was prepared as an account of work sponsored by the United States Government. While this document is believed to contain correct information, neither the United States Government nor any agency thereof, nor the Regents of the University of California, nor any of their employees, makes any warranty, express or implied, or assumes any legal responsibility for the accuracy, completeness, or usefulness of any information, apparatus, product, or process disclosed, or represents that its use would not infringe privately owned rights. Reference herein to any specific commercial product, process, or service by its trade name, trademark, manufacturer, or otherwise, does not necessarily constitute or imply its endorsement, recommendation, or favoring by the United States Government or any agency thereof, or the Regents of the University of California. The views and opinions of authors expressed herein do not necessarily state or reflect those of the United States Government or any agency thereof or the Regents of the University of California.

UCRL-17212
Preprint

Submitted to: Acta Metallurgica

UNIVERSITY OF CALIFORNIA

Lawrence Radiation Laboratory
Berkeley, California

AEC Contract No. W-7405-eng-48

DEFORMATION AND FRACTURE OF GOLD-PLATINUM POLYCRYSTALS STRENGTHENED BY SPINODAL DECOMPOSITION

Ray W. Carpenter

November 1966

DEFORMATION AND FRACTURE OF GOLD-PLATINUM POLYCRYSTALS STRENGTHENED BY SPINODAL DECOMPOSITION

Ray W. Carpenter*

Inorganic Materials Research Division, Lawrence Radiation Laboratory,
Department of Mineral Technology, College of Engineering,
University of California, Berkeley, California

November 1966

ABSTRACT

The plastic deformation and fracture characteristics of two gold-platinum alloys strengthened by spinodal decomposition have been experimentally investigated. It was found that the fracture path in these alloys is primarily intergrannular; this is caused by incoherent grain boundary precipitation of the equilibrium phases. The grains themselves are not embrittled by the transformation. It was also found that the initial work-hardening rate is higher than normally observed, and that the proportional limit is appreciably increased by spinodal decomposition. A new theory was advanced to account for the work-hardening behavior, and it is in good agreement with experimental results. It was also shown that present theories cannot account for the large increase in proportional limit.

---

* Now at Oak Ridge National Laboratory, Oak Ridge, Tenn.

INTRODUCTION

Non-ferrous precipitation-hardening alloys generally exhibit maximum strength during the early stages of the precipitation reaction, when in the stage of coherent preprecipitation. The preprecipitates should not be more than about 100 Å apart, and should be as uniformly distributed through the volume as possible.(1)

Spinodal decomposition* is a method of obtaining such a structure. Early investigations of this mechanism implied that it is the closest approach to homogeneous nucleation in the solid state.(2) Later experimental investigations of face-centered cubic alloys of this type showed that structural changes occurring within the unstable solution lattice consisted of clusters leading to precipitates of the equilibrium phases and were distributed periodically in the parent lattice, the periodicity being along the cube axis directions.(3,4,5) Recent theoretical treatments of spinodal decomposition(6,7) lead to the same conclusion, i.e., that the spatial distribution of "nuclei" should be periodic within the parent lattice. In particular, Cahn's theoretical treatment for cubic alloys includes the effect of elastic strain energy in the criteria for existence of spinodal decomposition and subsequent growth of the structure; an important conclusion was that wave propagation vectors should be in the cube axis directions for spinodal gold-platinum alloys, producing a uniform preprecipitate dispersion.

---

* Spinodal decomposition is thought to occur within the spinodal region of a two-phase field, where the boundary of the chemical spinodal region is defined by the locus of $\frac{\partial^2 F}{\partial X^2} = 0$: F = Gibbs free energy of the unstable solution and X = atom fraction in a binary alloy.

Tiedema, et al.[5] investigated the spinodal reaction in the gold-platinum system by x-ray diffraction methods and found that the maximum wavelength (characterizing the periodic cluster distribution) attained before loss of coherency was about 40 a_o, where a_o is the lattice constant of the unstable solution. Measurements of microhardness were made on alloy specimens at various stages of isothermal aging; very high values were attained (up to ~450 vickers) and occasionally brittle-type fractures occurred, so it appeared that spinodal decomposition may have caused marked changes in mechanical properties of the alloys.

The present research was undertaken to investigate in detail the deformation and fracture characteristics of gold-platinum alloys isothermally aged within the spinodal region of the phase diagram. Of particular interest is the reported brittle nature of these alloys, which was attributed to quenching strains by earlier investigators. Preliminary results of the present work indicated that the apparent brittle fracture is caused by grain boundary precipitation.[8]

EXPERIMENTAL METHOD

Alloy specimens of nominal compositions 60% Au-40% Pt and 20% Au-80% Pt* were supplied in the form of 0.020 inch diameter wire, fabricated from induction melted ingots in the manner previously described.[9]

Spectroscopic analysis for metallic impurities showed the major contaminants to be Rh(<.04%), Pd(<.07%), Fe(<.07%); all others less than 0.01%. Particular attention was given to silicon concentration;

*weight percent, hereafter called 40-60 and 80-20, respectively.

two separate determinations showed silicon concentration to be < 0.0005%.

The wire tensile specimens were homogenized by direct resistance heating for 1 hour at 1225 ± 5°C followed by He gas quenching to room temperature. Isothermal aging at 510 ± 10°C was done in either a molten salt bath followed by ice water quenching, or in the same manner as homogenization. Both of these operations have been described in detail earlier.(9)

Because of limited ductility found in aged specimens it was necessary to devise a gripping technique that would not deform the wires at the points of contact. The grips developed are shown disassembled with the alignment jig in Fig. 1a and assembled in Fig. 1b. The tensile specimens were epoxy resin bonded in the small stainless steel grip tubes with snap rings fitted on each end. The larger brass grips, with threaded ends for attachment to the testing machine, were drilled and broached to provide a slip fit with the stainless steel tubes. The snap rings anchored the grip tubes in the brass grips. The tensile specimens were 3.25 in. overall and the gripped length was about 0.875 in. on each end. The free span between brass grips was about 1.5 in. The assembled tensile specimen and grip assembly was placed in the aluminum alignment jig, as shown in Fig. 1b, before the resin was cured. With the alignment jig fastened shut, so that the whole specimen-grip assembly was a rigid unit, the resin was cured at 60°C. The jig was not removed until the specimen was in the tensile machine, with a slight preload applied.

Tensile tests were made in an Instron constant strain-rate testing machine. All tests were performed at a constant strain rate of 0.005 in. per min. Specimen elongation was measured directly, using the central inch of the specimen free span as a guage length, by attachment of an

electrical extansometer (Instron Model No. G-51-11, sensitivity 5×10^{-5} inch) directly on the wire; experimental results were displayed directly as a load-strain curve. Calibration of the extensometer with a micrometer head showed that a displacement of 5×10^{-5} in. could be reproducibly measured. The calibration of the load cell and extensometer system was checked with music wire specimens; the average elastic modulus was calculated to be $29.0 \pm 0.5 \times 10^{6}$ psi for five determinations.

EXPERIMENTAL RESULTS

Characteristic stress-strain curves of 40-60 alloys in the homogenized and quenched condition and after aging for various times are shown in Figs. 2 through 5. Mechanical properties of these alloys determined from the stress-strain curves are given in Table I.

TABLE I

Mechanical Properties for 40-60 Alloys Aged at 510°C

Age Time Hours	Youngs Modulus $10^{-6} \times$ psi	Proportional Limit** $10^{-3} \times$ psi	Fracture Stress $10^{-3} \times$ psi	Plastic Strain $\times 10^{3}$
0*	21.6	74	121	32.3
0.5	20.5	95	160	4.20
1*	19.2	96	162	4.05
5*	20.9	110	161	2.65
10*	21.4	110	169	2.98
20*	21.1	110	169	3.02
97.5*	21.6	109	166	2.98

* Duplicate specimens.

** Proportional limit defined as stress corresponding to departure from linearity on stress-strain curve.

The most pronounced change accompanying aging was the large increase in work hardening rate and the abrupt decrease in plastic strain to fracture evident from the beginning of the precipitation reaction. The initial yield point increases by about 25% during the first one-half hour of aging and approaches a constant value about 50% higher than the homogenized and quenched alloy after 5 hours aging at 510°C. Another group of specimens was aged at 410°C to investigate mechanical property changes at earlier stages of the reaction. The results obtained are given in Table II and characteristic stress-strain curves for two of the alloys are shown in Figs. 6 and 7.

Table II

Mechanical Properties of 40-60 Alloys Aged at 410°C

Aging Time Hours	Youngs Modulus 10^{-6} psi	Proportional Limit 10^{-3} psi	Fracture Stress 10^{-3} psi	Plastic Strain to Fracture $\times 10^{3}$
5	20.6	96	150	5.57
10	22.0	96	155	4.80
40	21.0	111	167	3.90
200*	20.8	102	160	3.04

* Duplicate specimens

The stress-strain curves for alloys aged at 410°C show the same general characteristics as those for alloys aged at 510°C, except that the increase in slope proceeds at a smaller rate. The average elastic modulus for all 40-60 specimens tested was $21 \pm 1 \times 10^{6}$ psi.

The work-hardening rate, defined here as the slope of the stress-strain curve at a specified plastic strain, was calculated graphically

for all stress-strain curves at a plastic strain of 2.5×10^{-3}. The selection of this strain value is arbitrary; it was chosen because it is the largest plastic strain allowing the rate calculation before fracture for all the stress-strain curves, and the slope of the curves become increasingly different at increasing strains. The results of these calculations are given in Table III; they show a gradual increase in work-hardening rate for the specimens aged at 410°C and a less well-defined increase for those aged at 510°C. The work-hardening rates at a plastic strain of 2.5×10^{-3} range from about 0.2E in the case of the homogenized and quenched specimens up to a constant value of about 0.85E.

TABLE III

Work-Hardening Rates of 40-60 Alloys Measured at Plastic Strain = 2.5×10^{-3} for Various Aging Times and Temperatures

Age Temperature °C	Age Time Hours	$d\sigma/d\epsilon$ $\times10^{-6}$ psi
0*	0	~ 4
410	5	10.1
410	10	12.0
410	40	14.4
410*	200	17.6
510	0.5	16.4
510	1	15.8
510	5	19.0
510*	10	18.3
510*	20	18.5
510*	97.5	17.7

* Avg. values for duplicate specimens

A number of tensile tests were conducted on quenched specimens of the 80-20 alloy. This alloy always fractured while still in the elastic region of the stress-strain curve. Fracture strengths were on the order of 130,000 psi. No further mechanical property tests were carried out on this alloy.

Tensile specimen fracture surfaces were examined optically using a scanning electron microscope. Fracture topology for specimens aged 1 hr at 510°C indicated that separation along grain boundaries was the primary failure mechanism. An example of this behavior is shown in Fig. 8. For a small central area of the wire the fracture path was transgranular, but most of the fracture was intergranular. This fracture behavior persisted in aged specimens up to the longest aging times investigated, as shown in Figs. 9 and 10. It has been shown earlier, by optical metallography, that incoherent grain boundary precipitation occurs in these alloys in small amounts during quenching from the homogenization temperature, and continues during aging.[5,8] When the alloys are in the homogenized and quenched condition grain boundary precipitation in the 80-20 alloy is easily observed, particularly at grain edge intersections, but it is almost absent in homogenized and quenched 40-60 alloys. Precipitate was easily observable in the intergranular region of fractures in aged specimens. A typical example is shown in Fig. 11, where a grain boundary precipitate about 2μ thick can be seen, as a vertical layer, defining the plane of intersection of two grains at the fracture surface. The amount of precipitate at grain boundaries is quite variable from one position in a specimen to another, some boundaries not exhibiting appreciable precipitate even after aging 100 hours at 510°C. Even small amounts of grain boundary precipitate will, however, have a noticeable

effect on the fracture surface appearance, as shown in Fig. 12. This homogenized and quenched 40-60 specimen fractured with about 50% reduction in area, but a few large, flat areas resulting from tearing along grain boundaries are present.

The flat grain boundary facets on fracture surfaces were examined for the presence of river markings characteristic of cleavage fracture, but none were found. The transgranular regions of the fractures, in the central parts of the wires, were also examined at higher magnification to determine the nature of the fracture there. These parts of the fractures were found to be composed of many very small cavities surrounded by what appeared to be small shear lips. An example of this is shown in Fig. 13. This is the characteristic appearance of a transgranular shear fracture in the scanning electron microscope.

An optical examination to determine the presence of slip within grains was made on the surface of several tensile specimens which had been electropolished before straining. Slip traces were found on many grains along each specimen examined; an example is given in Fig. 14. Slip traces were generally quite difficult to observe optically. Usually long, straight slip lines in a single direction (in a particular grain) were observed. In grains forming the fracture surface coarse slip bands were observed, as shown in Fig. 15. Several specimens were examined by sectioning along the wire axis after tensile testing to determine whether multiple cracking of grain boundaries had occurred during tensile testing, but no evidence of this type of failure was found.

It has been shown by earlier microhardness measurements that the grain boundary precipitate is softer than the grains themselves, but it was not possible to measure the difference quantitatively because of

the small boundary thickness.[8] Some qualitative investigations of the composition of the grain boundary precipitate were made with a microprobe. These were generally inconclusive until relatively thick regions were formed. These regions appeared to be platinum rich relative to the grain interiors in 40-60 alloys.

DISCUSSION

Fracture Characteristics

The brittle appearing grain boundary fractures are unusual in an alloy of two elements normally considered quite ductile whose phase diagram exhibits no ordered phases or intermetallic compounds.[14] It was reported earlier that the brittle grain boundary fracture characteristic appeared to results from a precipitation in the grain boundaries of a thin film of soft nearly equilibrium phase material weaker than the grains themselves.[8] The precipitate was expected to be platinum-rich in 40-60 alloys and gold-rich in 80-20 alloys. The present microprobe results substantiate this conclusion for 40-60 alloys aged for long times at 510°C. Microprobe results for both alloys aged for short times were inconclusive. 20-80 alloys were not examined after long aging times.

The question of whether or not plastic straining in the grain boundaries makes a significant contribution to the observed plastic strain during a tensile test must be considered. In the homogenized and quenched 80-20 alloys metallographic observation showed grain-boundary precipitation to be present, but no measureable strain was observed upon testing. In aged 40-60 alloys the amount of grain-boundary precipitate increased with aging time, but the plastic strain to fracture decreased until maximum strength was reached and remained nearly constant thereafter (Table I). These experimental observations make it unlikely that significant plastic strain

could result from flow of precipitate in the grain boundaries. The absence of multiple grain-boundary cracking along the length of the specimen noted above precludes this phenomenon as a source of apparent plastic strain.

It is concluded that fracture occurred in the grain boundaries because of the soft material present there and appeared to be brittle because the much stronger surrounding grains constrained the softer phase in the boundaries and prevented its flow.

Work-Hardening Behaviour

The high work-hardening rate observed during tensile testing of aged 40-60 alloys extended to strains larger than 0.25% into the plastic region of the stress-strain curve. The observed rate is too large to be accounted for by existing theories of work-hardening, and the high rate persists over larger plastic strains than the usual extent of the initial steep part of a stress-strain curve for a polycrystal (Stage II). The stress-strain curves for soft copper, iron, and tantalum wires, determined in the same way as for the gold-platinum alloys, showed that the Stage III work-hardening rate was always well established after about 0.1% plastic strain; the amount of plastic strain required to re-establish the Stage III work-hardening rate was much less than 0.1% when the specimens had been previously strained into the Stage III region.

The high work-hardening rates observed in the present work could be accounted for by a structural model based on results of earlier x-ray diffraction and theoretical investigations of the transformation mechanism.[5,7,10]

The structural changes occurring in the supersaturates solution lattice of alloys undergoining spinodal decomposition cause a diffuse scattering phenomenon termed "sidebands" to appear on x-ray diffraction photographs taken during the early stages of the reaction. The theoretical treatments of sideband scattering noted above indicate that its origin is a periodic modulation of the lattice constant of the supersaturated lattice, in the cube axis directions.[3,5] A "wavelength" characteristic of the size of the lattice parameter modulations can be calculated from the Daniel-Lipson equation:

$$\lambda = \frac{h \tan \theta_{hkl}}{(h^2 + k^2 + l^2)\Delta\theta} \qquad (1)$$

where

λ = modulation wavelength, in lattice parameters of the quenched metastable solution

h,k,l = Miller indices of parent Bragg reflection

θ = Bragg angle of parent reflection

$\Delta\theta$ = angular displacement of sidebands from θ

for a Bragg line with indices of the form (h h h), (h h 0) or (h 0 0).

An investigation of the variation of wavelength with isothermal annealing time has been made for several gold-platinum alloys; the results for the 40-60 alloy at 502°C show the wavelength to vary logarithmically with aging time (see Fig. 16). The initial wavelength is about $17a_o$ and this increases to about $35a_o$ in 1200 min.[9] It is assumed that the lattice parameter is modulated along the three cube axes. Along one axis the modulation is given by

$$a = a_o + \frac{\Delta a}{2} \sin\pi \frac{x}{(\lambda/2)} \qquad (2)$$

where

a_o = lattice constant of the quenched solution

Δ_a = maximum difference in lattice constant between gold-rich and and platinum-rich regions

λ = wavelength of alloy in lattice constants of quenched solution.

The alloy lattice is considered to be a sequence of alternating gold and platinum-rich regions along ⟨100⟩ in space, with average spacing between centers of $\lambda/2$. The movement of dislocations under an externally applied stress will cause lattice mismatch shearing strains, for example, by shearing a platinum-rich region over a gold-rich region. One slip system of the form {111} ⟨1$\bar{1}$0⟩ is assumed active per grain. The maximum shear strain possible is $\frac{\Delta a}{2a}$. The lattice shear strain caused by the passage of n dislocations through the lattice can be represented by the following equation, when nb is small compared to λ:

$$\gamma = \gamma_{max} \cdot y \sin \frac{2\pi nb}{\lambda} \tag{3}$$

where y is a unit vector in the slip direction. If $\lambda' \equiv \lambda/|b|$ and noting that $\gamma_{max} = \frac{\Delta a}{2a_o}$ then the lattice disregistry shear strain is

$$\gamma = \frac{\sqrt{2}a}{2a_o} \sin \frac{2\pi n}{\lambda'} \tag{4}$$

The tensile stress, T, opposing the further propagation of dislocations through the lattice (assuming Schmid factor = 1/2) is

$$T \cong \frac{\sqrt{2}\,\Delta a}{a_o} G \sin \frac{2\pi n}{\lambda'} \tag{5}$$

and the total flow stress for the alloy in the plastic region is

$$\sigma_T = \sigma_{PL} + \frac{\sqrt{2}\,\Delta a}{a_o} G \sin\left(\frac{2\pi n}{\lambda^2}\right) \qquad (6)$$

where σ_{PL} is the stress at the experimentally observed proportional limit, and G is the shear modulus. G is calculated to be 7.5×10^6 psi from the experimental value $E = 21 \times 10^6$ psi, assuming $\nu = 0.4$. The lattice constant, a_o, for the unstable solution is 4.015Å, and the difference in cubic lattice constants of the equilibrium phases is 0.123Å.[9] The equilibrium value of Δa is however, not the correct value to use in Eq. (5); it is too large for the coherent state. An approximate calculation of the coherent Δa, which is unavailable from x-ray diffraction or thermodynamic measurements on gold-platinum alloys, can be made from x-ray measurements of spinodal decomposition in other alloys.

Guinier[11] has pointed out that alloys exhibiting sidebands in the early stages of precipitation reactions may have intermediate stages in the precipitation reaction between the sideband and equilibrium stages; the occurrence of such intermediates is related to the difference in lattice constants of the cubic equilibrium phases. For example, iron-copper-nickel spinodal alloys exhibit an intermediate stage of two coexisting tetragonal phases between the sideband and equilibrium stages;[4] in this case the difference in equilibrium cubic lattice constants is ~1%, compared to 3.4% for gold-platinum alloys. Gold-nickel alloys have ~10% difference in equilibrium lattice parameters, and it is very difficult to obtain even the initial sideband stage in the precipitation reaction.[12] It is reasonable to assume that the existence of the modulated structure depends on the strain-energy associated with it; the strain energy will increase as Δa increases toward the equilibrium value and the occurrence of intermediate stages beyond sidebands depends on the difference of atomic

diameters of the constituent atoms. If this difference is too large, the different c/a values of the coexisting tetragonal phases will prevent their formation and the cubic equilibrium phases appear directly. The maximum coherent value of the cubic lattice constant modulation can be calculated from the measured lattice constants of the coexisting tetragonal "phases" for iron-copper-nickel alloys by assuming the volume of the tetragonal cells is the same as the modulated cubic cells that preceded them. Hargreaves[4] measured the lattice constants of the partially coherent coexisting tetragonal phases in an iron-copper-nickel spinodal alloy ($Cu_{10}Fe_7Ni_3$); the calculated maximum Δa for the cubic modulations is 0.023Å and the lattice constant of the quenched solution is 3.586Å. The coherent Δa for gold-platinum modulated structures is estimated to be:

$$\Delta a_{Au\text{-}Pt} \cong \Delta a_{Fe\text{-}Cu\text{-}Ni} \left(\frac{a_{o_{Au\text{-}Pt}}}{a_{o_{Fe\text{-}Cu\text{-}Ni}}} \right) = 0.026\text{Å} \qquad (7)$$

This calculation neglects differences in elastic moduli between the two systems, however a recent estimate shows they probably do not differ by more than ~15%, which is negligible for the present purposes.[13]

If it is assumed that active slip planes in this alloy are ~1μ apart and G is taken to be 7.5×10^6 psi as calculated above, a stress-strain curve can be calculated. This has been done for an alloy having a wavelength of 40b, corresponding to an aging treatment of ~10 hours at 510°C. The results are compared with the stress-strain curve in Fig. 17. Calculated values agree quite closely with the experimental curve.

Proportional Limit

The experimental results show that the proportional limit increases with aging time in the 40-60 alloys. It is interesting to compare the present results with a theoretical treatment of strengthening by spinodal decomposition due to Cahn.[15] He assumes infinitesimal periodic composition fluctuations along cube axes of the form

$$C - C_o = A \sin \frac{2\pi x}{\lambda} \tag{8}$$

where

C = $C(x)$
x = distance along cube axis
C_o = average alloy composition
A = amplitude of fluctuation
λ = fluctuation wavelength

The various contributions to the forces on a stationary dislocation in equilibrium with its environment (i.e., before application of external stress) are considered and the tesselated stress field caused by the periodic variation in lattice constant (resulting from the composition fluctuations) is found to be predominant. For a (111) [1$\bar{1}$0] slip system in a face-centered-cubic alloy, a string model of a dislocation is allowed to assume its equilibrium shape in the stress field. Two cases are examined:

1) If the dislocation is very flexible, it can bend around energy hills of the stress field and loop between them. This behavior is analogous to Orowan hardening.
2) If the dislocation is stiff (or the stress field fluctuates steeply on a small scale) it must remain nearly straight and shear the composition fluctuations when moving under an applied stress.

Case 2 above should hold if the inequality holds,

$$\frac{A\eta bE\lambda}{2\pi Gb^2} < 1 \tag{9}$$

where A is as above in Eq. (8) and

b = Burgers vector

$\eta = \frac{d\ell na}{dC}$, a = lattice constant, C = C(x)

E = Young's modulus

G = Shear modulus

Expression (9) can be evaluated for the present case by noting that

$$A\eta = A\,\frac{d\ell na}{dC} \simeq \frac{A}{a}\,\frac{\Delta a}{\Delta C} = \frac{\Delta a}{2a_o}, \tag{10}$$

the same lattice strain parameter used in the discussion of work-hardening above. Now the criterion for shearing or non-shearing of the fluctuations becomes

$$\frac{\Delta aE\lambda}{4\pi a_o Gb} \simeq \frac{(.03)(21\times10^6)(40b)}{4\pi(4.015)(4)(7.5\times10^6)(6)} = 6.3\times10^{-2} < 1 \tag{11}$$

indicating that dislocations are nearly straight and shearing of the fluctuations should occur during plastic strain. This is consistent with the model described above for work-hardening. Now the applied stress necessary to cause yielding is given as

$$\sigma = \frac{(A\eta)^2E^2\lambda}{6\pi\sqrt{6}\,Gb} \tag{12}$$

for screw dislocations and

$$\sigma = \frac{(A\eta)^2E^2\lambda}{2\pi\sqrt{2}\,Gb} \tag{13}$$

for edge dislocations.

It is seen that screw dislocation should move most easily. The experimental results show that the proportional limit is ~10^5 psi for a 40-60 alloy with $\lambda \approx 40b$ (corresponding to about 10 hrs. aging at 510°C). Putting the values obtained earlier in Eq. (12) we calculate $\sigma \approx 600$ psi, considerably less than the experimental value. For edge dislocations the calculated yield stress is ~ 2800 psi.

It may be objected that the value of Δa, .03Å, estimated above is too low, causing an error in the calculated yield stress. However, assuming a yield stress of 10^5 psi and using Eq. (12), the value of Δa required to give a yield stress equal to that observed can be calculated. This was done, and the required $\Delta a = 0.35$Å. This is unrealistically high, since the difference in equilibrium cubic lattice constants is ~0.13Å. This yield stress theory is based on assumed infinitesimal composition fluctions, and is the equivalent of Mott-Nabarro hardening by long range coherency stresses in nucleation and growth age-hardening systems. In the present experiments the composition fluctuations are much larger than infinitesimal, and this may cause the disagreement. No further detailed analysis of the increase in proportional limit has been undertaken in the present work.

SUMMARY AND CONCLUSIONS

The changes in mechanical properties of two gold-platinum alloys due to spinodal decomposition have been determined experimentally. The proportional limit and initial work-hardening rate of 40-60 alloys increased upon isothermal aging within the spinodal region, and the fracture mode changed from ductile shear-type in the homogenized and quenched alloys to one of primarily grain-boundary character in the aged specimens. The 20-80 alloy exhibited the same fracture characteristics in the homogenized

and quenched condition; aged alloys of this composition were not investigated.

The grain-boundary fractures observed are caused by incoherent grain boundary precipitation of a second phase, different in composition from the matrix. For the 40-60 alloys, this phase is platinum-rich; according to the phase diagram it is nearly pure platinum, and therefore much softer than the surrounding hard matrix grains. The grain boundary precipitate should be gold-rich in the 20-80 alloys, and the grain boundary fracture occurs for the same reason as in the 40-60 alloys. Metallographic results showed that the grains themselves are not embrittled by the spinodal transformation.

The increase in work-hardening rate at small strains was analyzed using a model for the structural changes occurring during the early stages of spinodal decomposition that is in agreement with the results of earlier x-ray diffraction investigations. The increasing rate is attributed to rapidly increasing deformation-induced internal strains, resulting from shearing, by moving dislocations, of uniformly distributed composition fluctuations in the parent solution lattice. The slope of the stress-strain curve is determined by the trigonometric term of Eq. (6), and this is dependent on the small scale, periodic characteristics of the structural changes during spinodal decomposition, not on the magnitude of Δa. The work-hardening model does not allow for the increase of Δa up to its limiting value during aging. This increase will also raise the work-hardening rate. The increase in proportional limit was examined in terms of an existing theoretical model for yielding in a spinodally decomposed structure. The experimentally determined proportional limit is much higher than the theoretically calculated value, and it is suggested that

the discrepancy results from the limitation of the theoretical treatment to infinitesimal composition fluctuations. Some uncertainty is introduced into the above calculations because the specimens examined were polycrystalline. It is felt however, that the present conclusions are well substantiated by the gross differences between the theoretical and observed proportional limits, and the large differences between the work-hardening rates observed here and the rates normally cited for face-centered cubic metals (or alloys containing coherent precipitates).

ACKNOWLEDGEMENTS

This work was performed under the auspices of the Unites States Atomic Energy Commission.

The author is pleased to acknowledge the encouragement and guidance of Prof. Earl R. Parker during the course of this work. He would like to thank R. L. Brady and the Engineering Test Section of the Livermore Lawrence Radiation Laboratory for performing the difficult and tedious mechanical properties tests and Mr. T. Suganuma (JEOL) and Mr. P. Whitcomb (ENGIS) for assistance with the scanning microscope. Finally, he would like to acknowledge the valuable discussions and assistance of Dr. Azziz Ahmadieh.

REFERENCES

1. A. Kelly and R. B. Nicholson, Precipitation Hardening, in Prog. Mat. Sci. 10, 3 (1963) p. 149.

2. G. Borelius, Ann. Physik 28, 507 (1937) and Arkiv. Mat. Astron. 32A, 1 (1944).

3. V. Daniel and H. Lipson, Proc. Roy. Soc., A; 181, 368 (1943); Proc. Roy. Soc. A; 182, 378 (1944).

4. M. E. Hargreaves, Acta Cryst. 2, 259 (1949); Acta. Cryst. 4, 301 (1951).

5. T. J. Tiedema, J. Bouman, and W. G. Burgers, Acta. Met. 5, 310 (1957).

6. M. Hillert, Acta Met. 9, 525 (1961).

7. J. Cahn, Acta Met. 9, 795 (1961).

8. R. W. Carpenter, A. Ahmadieh, and E. R. Parker, Acta Met. 14, 543 (1966).

9. R. W. Carpenter, Growth of Modulated Structure in Gold-Platinum Alloys, to be submitted.

10. E. R. Parker, R. W. Carpenter, and V. F. Zackay, International Conference on Fracture, Sendai, Japan (1965).

11. A. Guinier, Solid State Physics, Advances in Research and Applications, Vol. 9, F. Sietz and D. Turnbull, Editors (Academic Press, New York, 1959).

12. R. M. Fisher and J. D. Embury, Electron Microscopy 1964, Vol. A. Proc. Third Eur. Reg. Conference, Prague (1964).

13. S. D. Dahlgren, private communication (1965).

14. A. S. Darling, R. A. Mintern, and J. C. Chaston, J. Inst. Metals, 81, 125 (1953-1953).

15. J. W. Cahn, Acta Met. 11, 1275 (1963).

FIGURE CAPTIONS

Fig. 1a Epoxy resin bonded tensile grips, shown disassembled with alignment jig.

Fig. 1b Tensile grips with fracture specimen mounted in open alignment jig.

Fig. 2 Stress-strain curves for 40-60 alloys aged at 510°C.

Fig. 3 Stress-strain curve for 40-60 alloy aged 1 hr. at 510°C.

Fig. 4 Stress-strain curves for 40-60 alloys aged 10 hrs. at 510°C.

Fig. 5 Stress-strain curves for 40-60 alloys after aging 20 hrs. at 510°C.

Fig. 6 Stress-strain curve for 40-60 alloy aged 40 hrs. at 410°C.

Fig. 7 Stress-strain curves for 40-60 alloys after aging 200 hrs. at 410°C.

Fig. 8 Fracture surface of 40-60 alloy tensile specimen aged 1 hr. at 510°C. 80×

Fig. 9 40-60 alloy tensile specimen fracture surface. Aged 97.5 hrs. at 510°C prior to test. 120×

Fig. 10 Fracture surface of 40-60 alloy tensile specimen aged 1 hr. at 510°C. 170×

Fig. 11 Grain-boundary precipitate at fracture surface of 40-60 alloy tensile specimen, aged 97.5 hrs. at 510°C prior to fracture. 1500×

Fig. 12 Small regions of grain-boundary fracture on tensile specimen of homogenized and quenched 40-60 alloy. 145×

Fig. 13 Appearance of central transgrannular region of fracture in 40-60 alloy tensile specimen, aged 5 hrs. at 510°C prior to fracture. 1850×

Fig. 14 Slip traces on grains in a 40-60 alloy tensile specimen. Tested after aging at 510°C. Grooves at grain boundaries are a result of the electropolishing technique. 1000×

Fig. 15 Coarse slip bands in grains on the fracture surface of a 40-60 alloy aged at 510°C prior to test. 1000×

Fig. 16 Variation in calculated structural modulation wavelength with isothermal aging time for 40-60 alloys.

Fig. 17 Comparison of experimental stress-strain curve with theoretical points for 40-60 alloy aged 10 hrs. at 510°C.

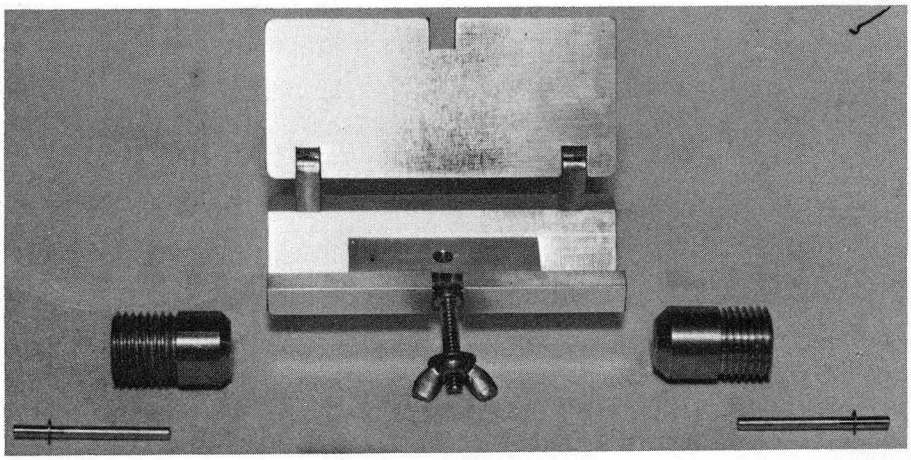

Fig 1a

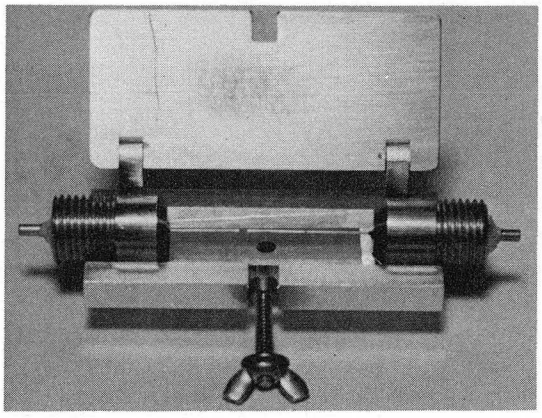

ZN-5786

Fig 1b

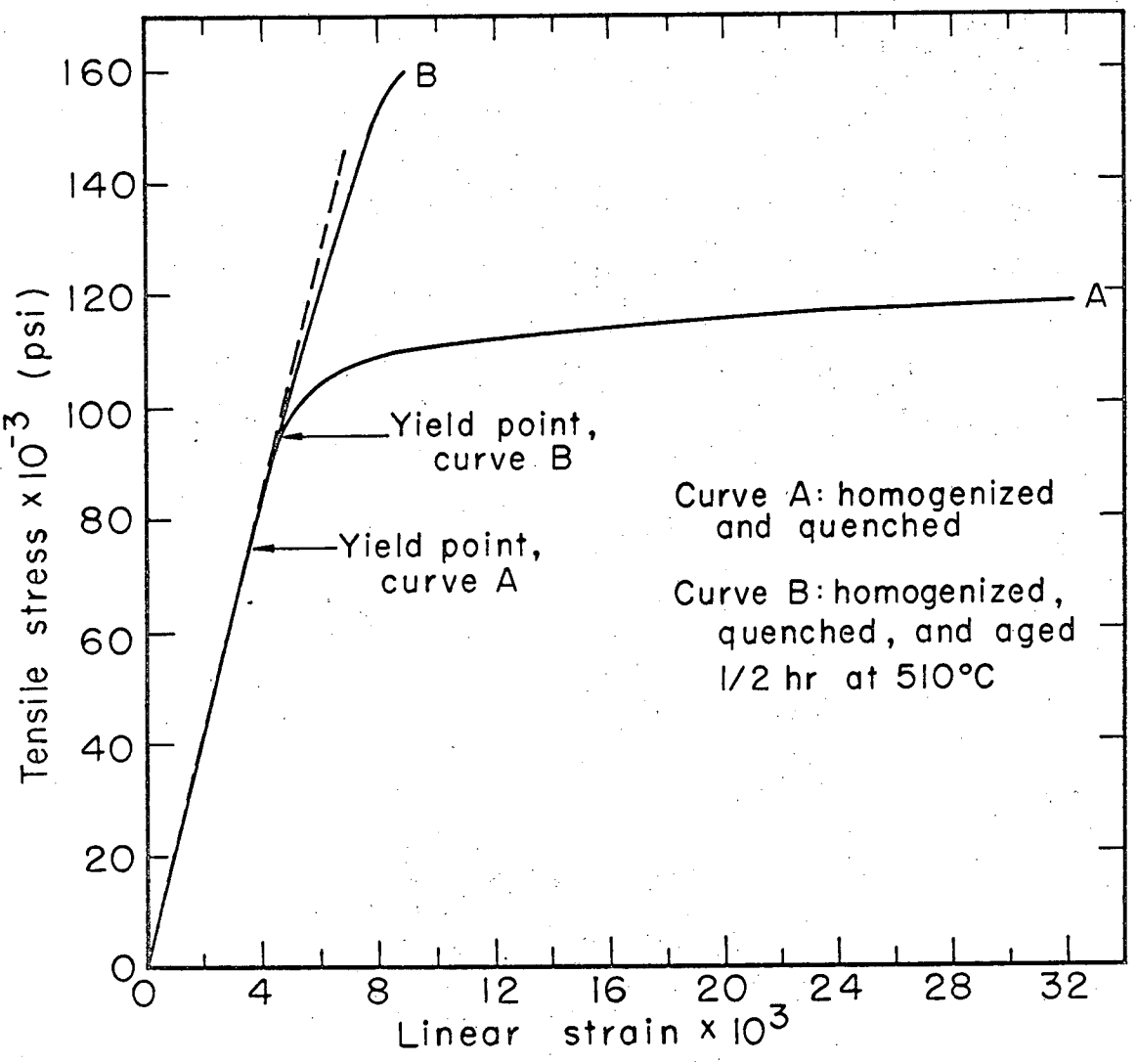

MU-37141

Fig. 2

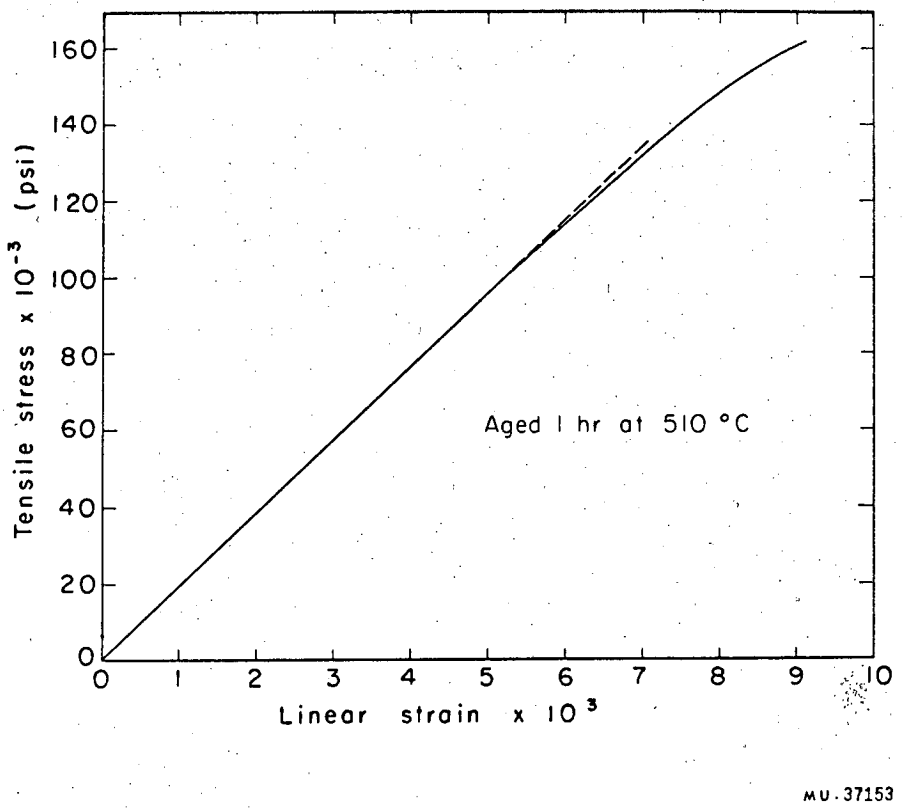
Tensile stress x 10^{-3} (psi)
160
140
120
100
80
60
40
20
0
0
1
2
3
4
5
6
7
8
9
10
Linear strain x 10^{3}
Aged 1 hr at 510 °C
MU-37153

Fig. 3

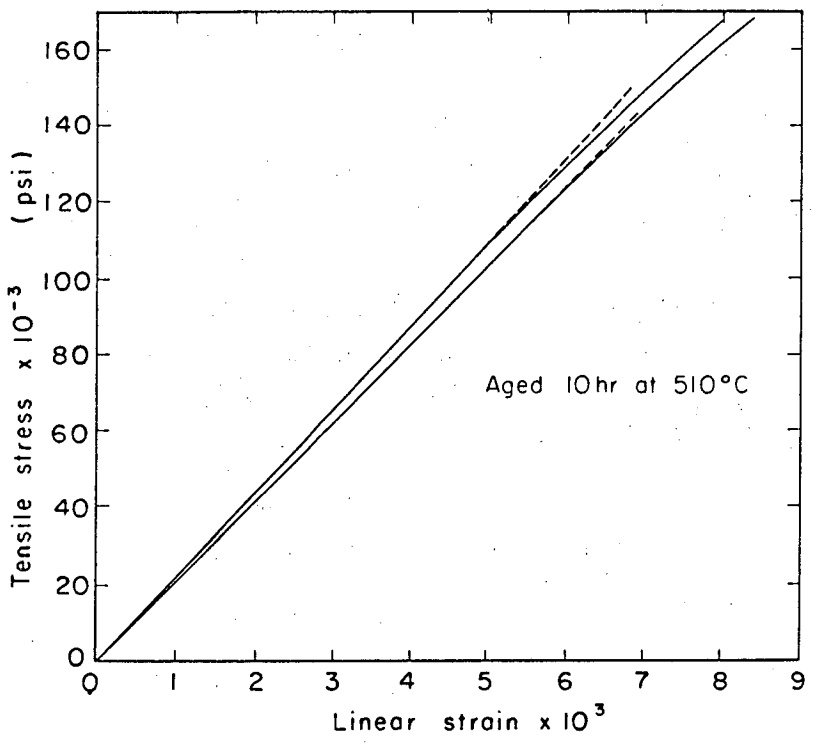
Tensile stress x 10^{-3} (psi)
160
140
120
100
80
60
40
20
0
0
1
2
3
4
5
6
7
8
9
Linear strain x 10^{3}
Aged 10 hr at 510°C
MU-37155

Fig. 4

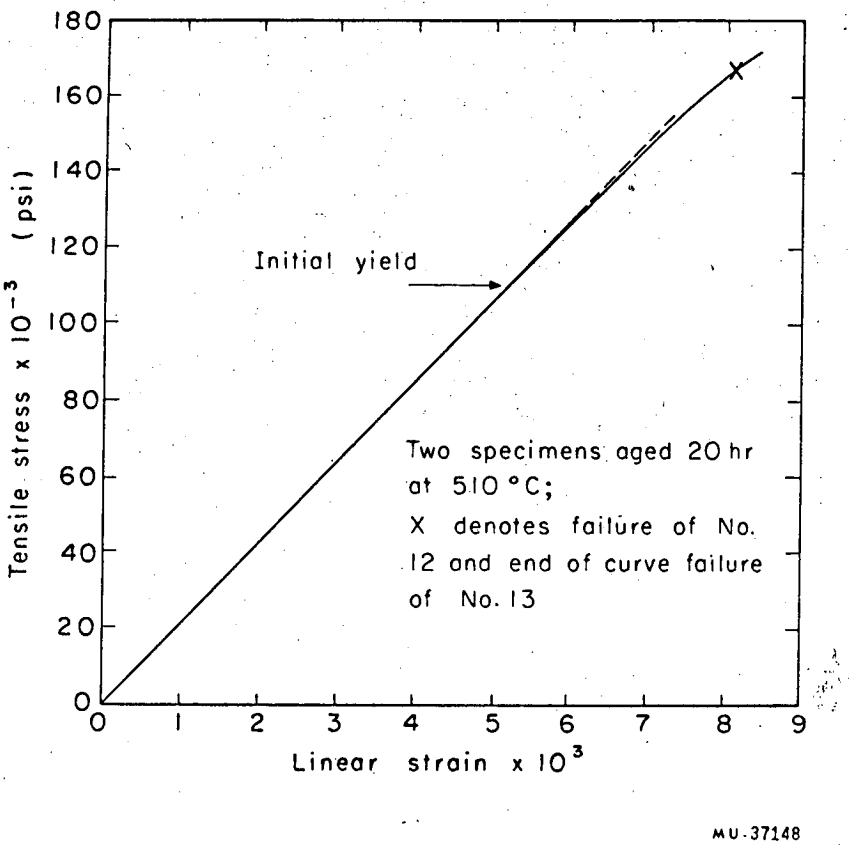
180
160
140
120
100
80
60
40
20
0
Tensile stress x 10^{-3} (psi)
0
1
2
3
4
5
6
7
8
9
Linear strain x 10^{3}
Initial yield
Two specimens aged 20 hr at 510 °C;
X denotes failure of No. 12 and end of curve failure of No. 13
MU-37148

Fig. 5

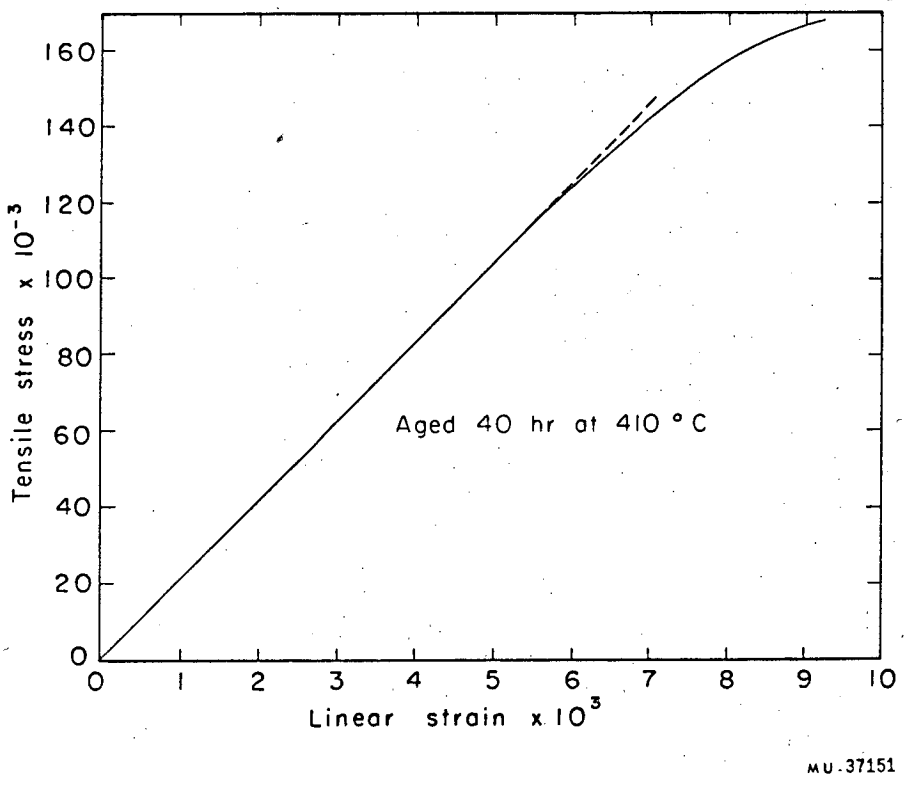
160
140
120
100
80
60
40
20
0
Tensile stress x 10^{-3}
0
1
2
3
4
5
6
7
8
9
10
Linear strain x 10^{3}
Aged 40 hr at 410 °C
MU-37151

Fig. 6

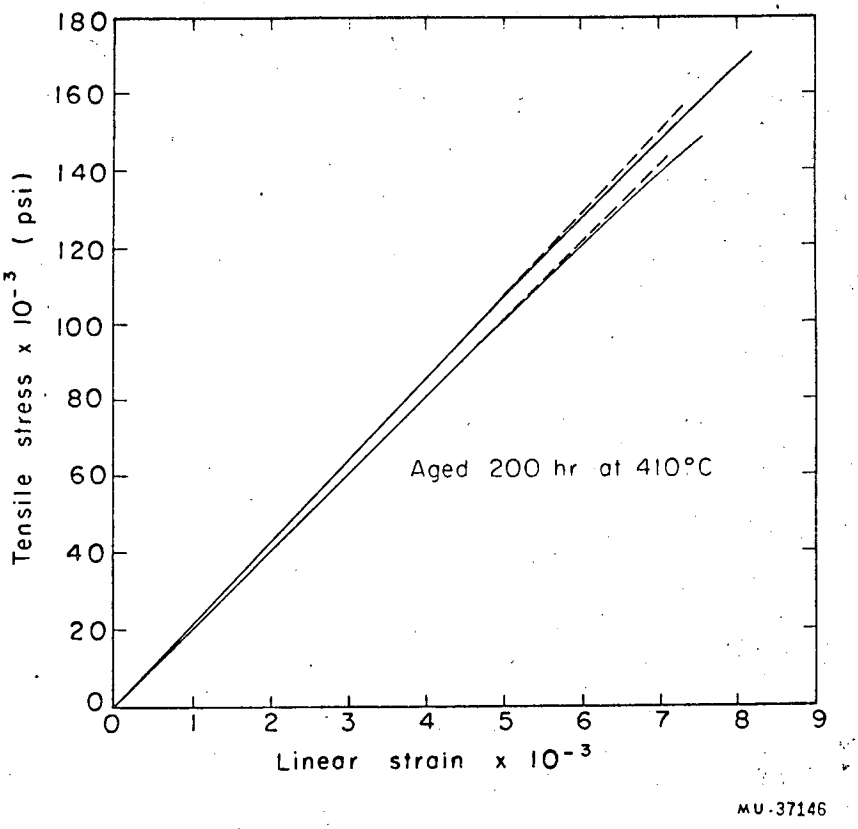
180
160
140
120
100
80
60
40
20
0
Tensile stress x 10^{-3} (psi)
0
1
2
3
4
5
6
7
8
9
Linear strain x 10^{-3}
Aged 200 hr at 410°C
MU-37146

Fig. 7

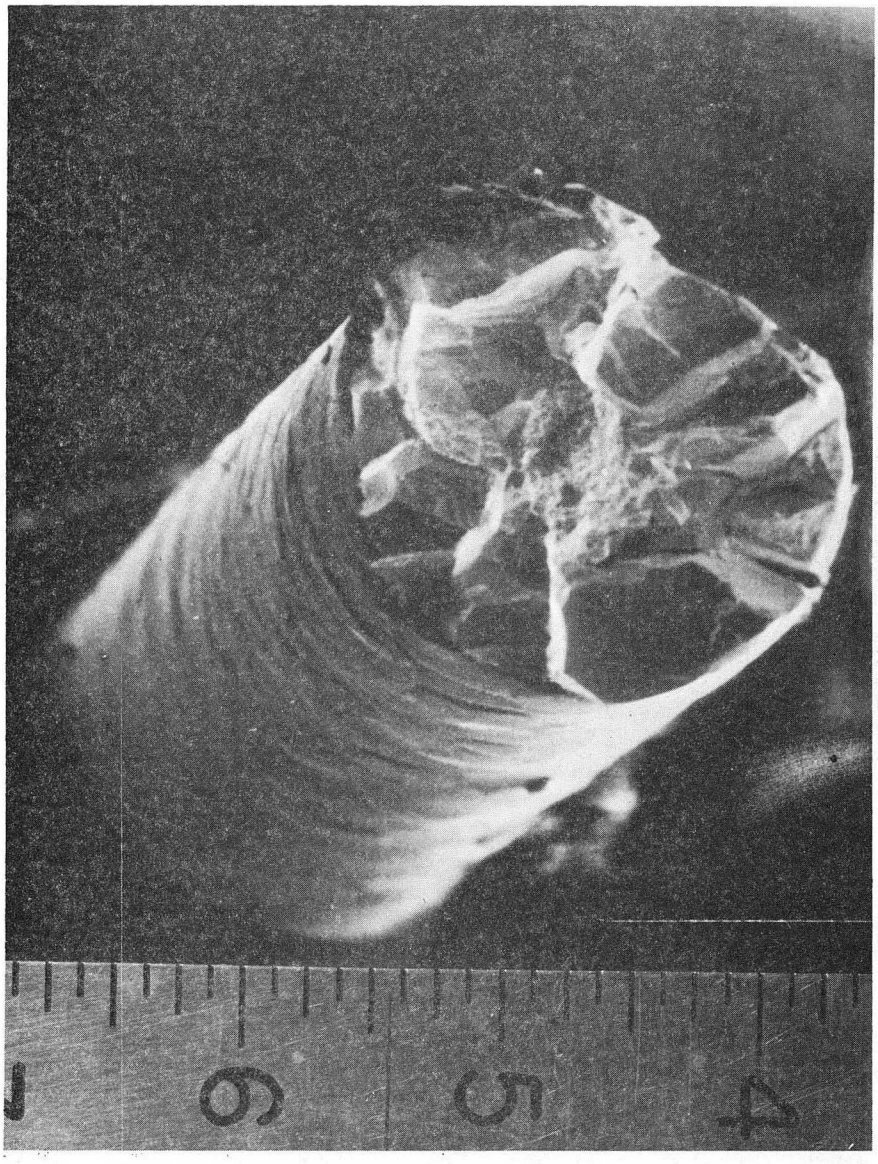

XBH671 14

Fig. 8

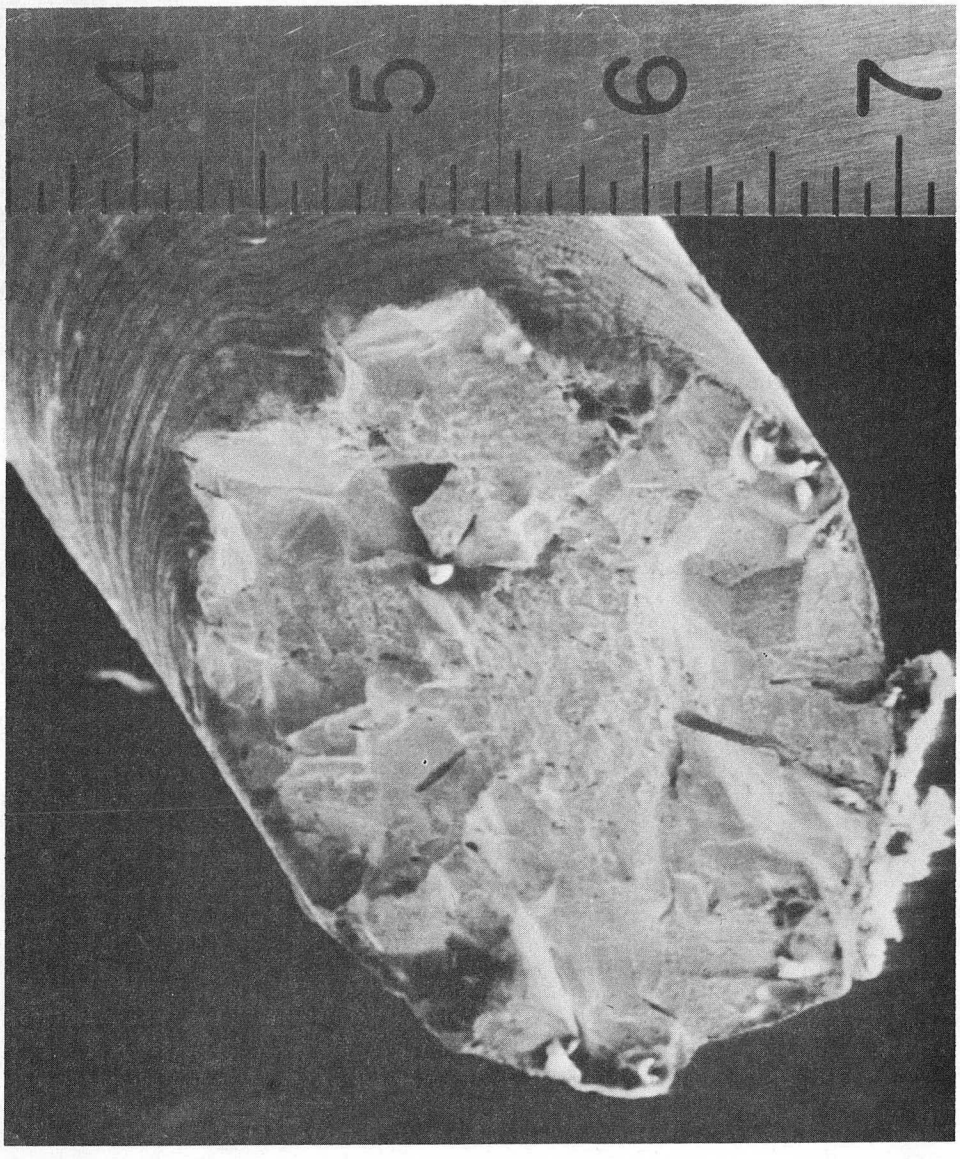

XBH671 15

Fig. 9

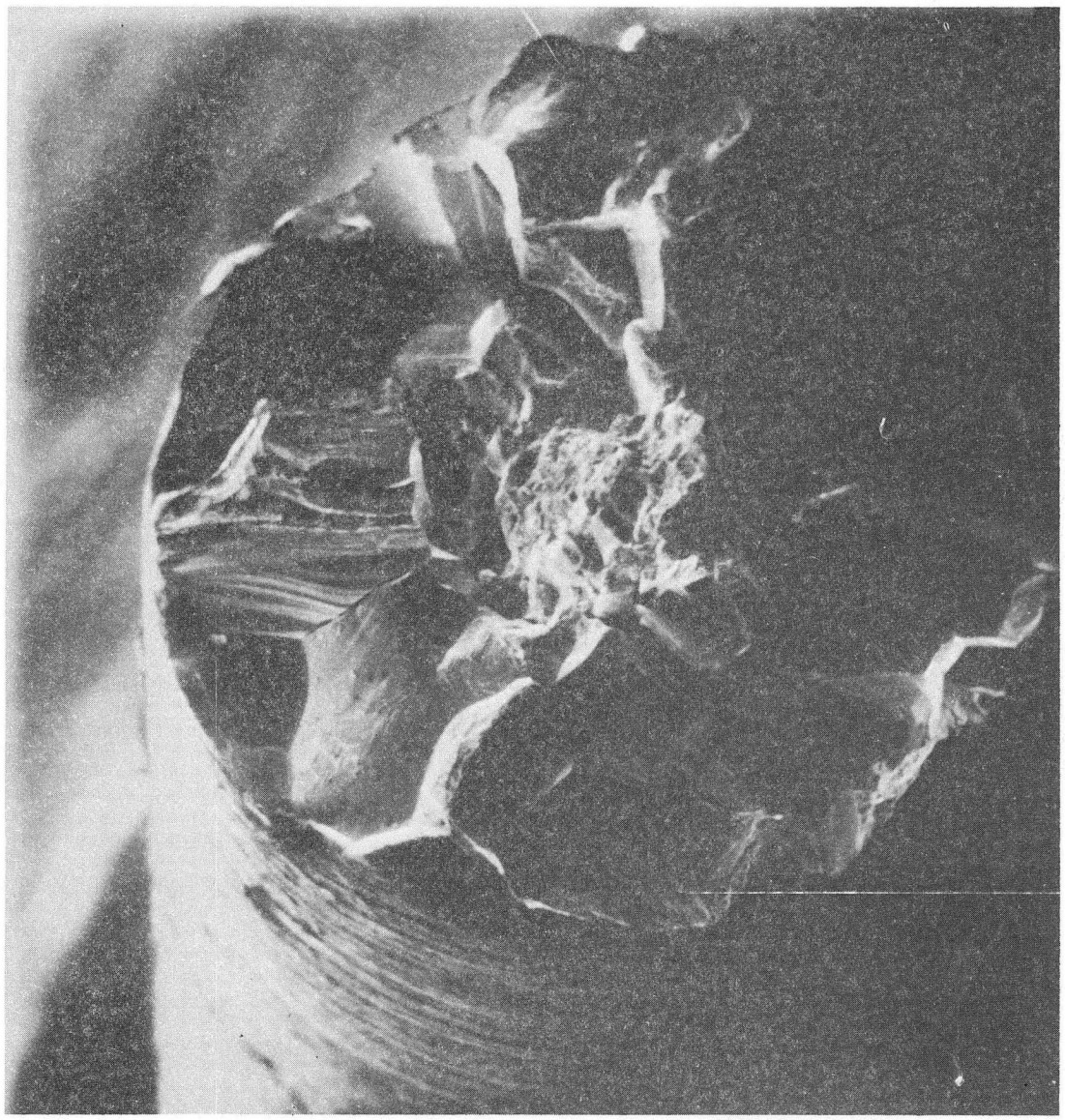

XBH671 16

Fig. 10

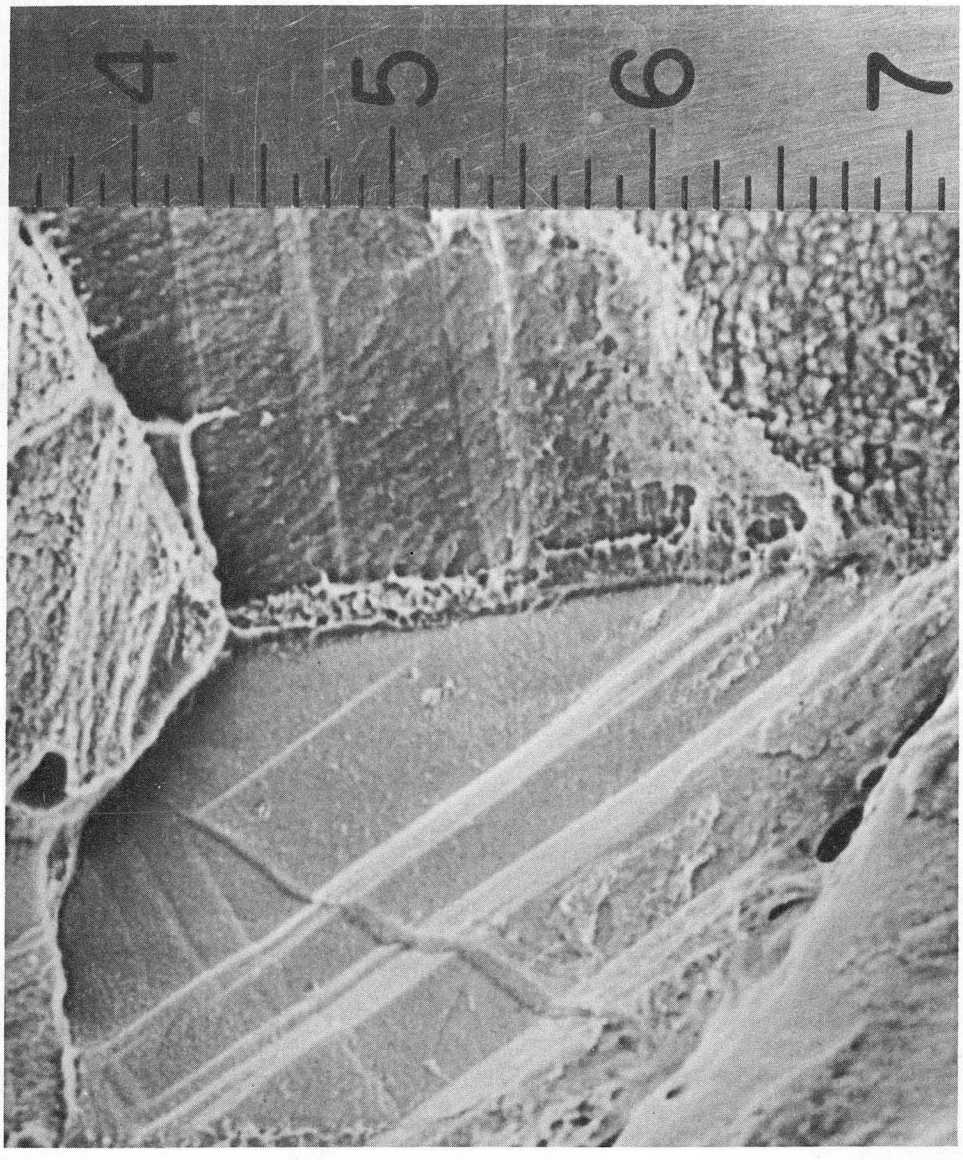

XBH671 17

Fig. 11

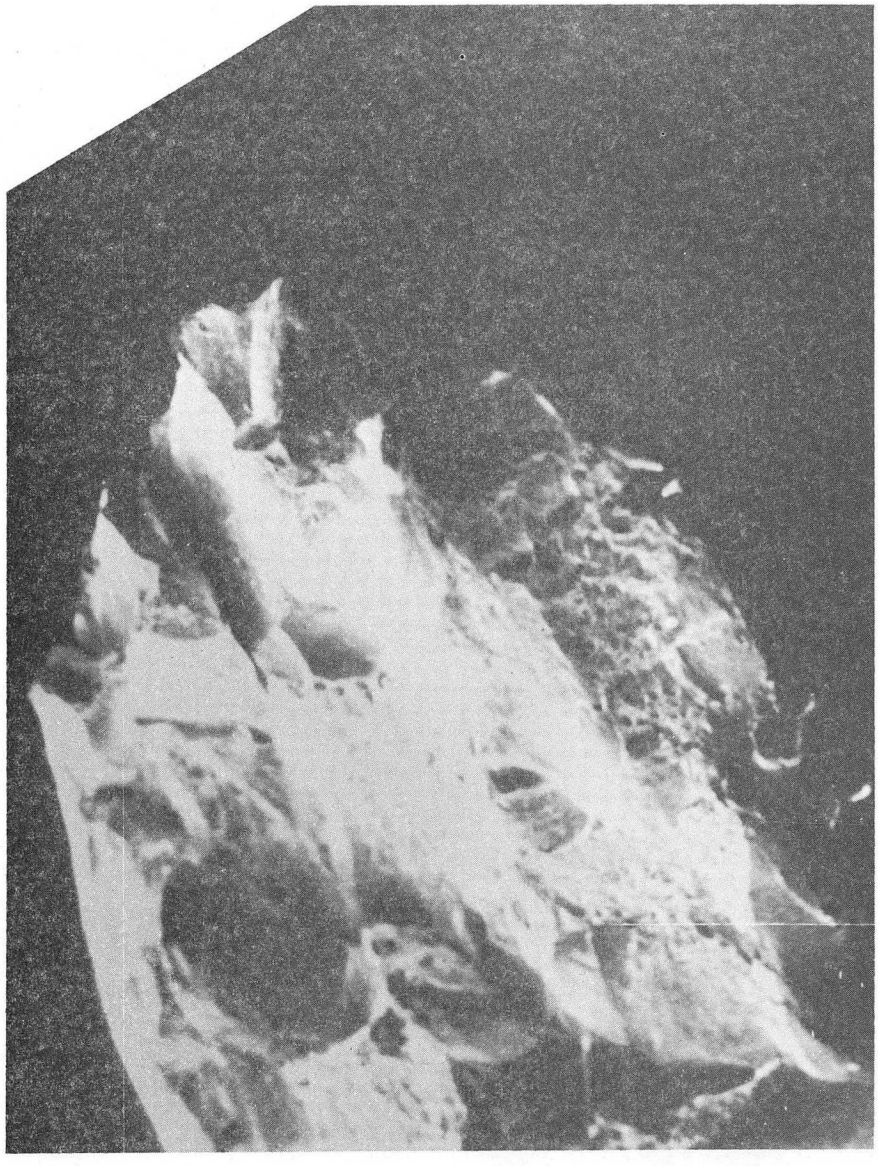

XBH671 18

Fig. 12

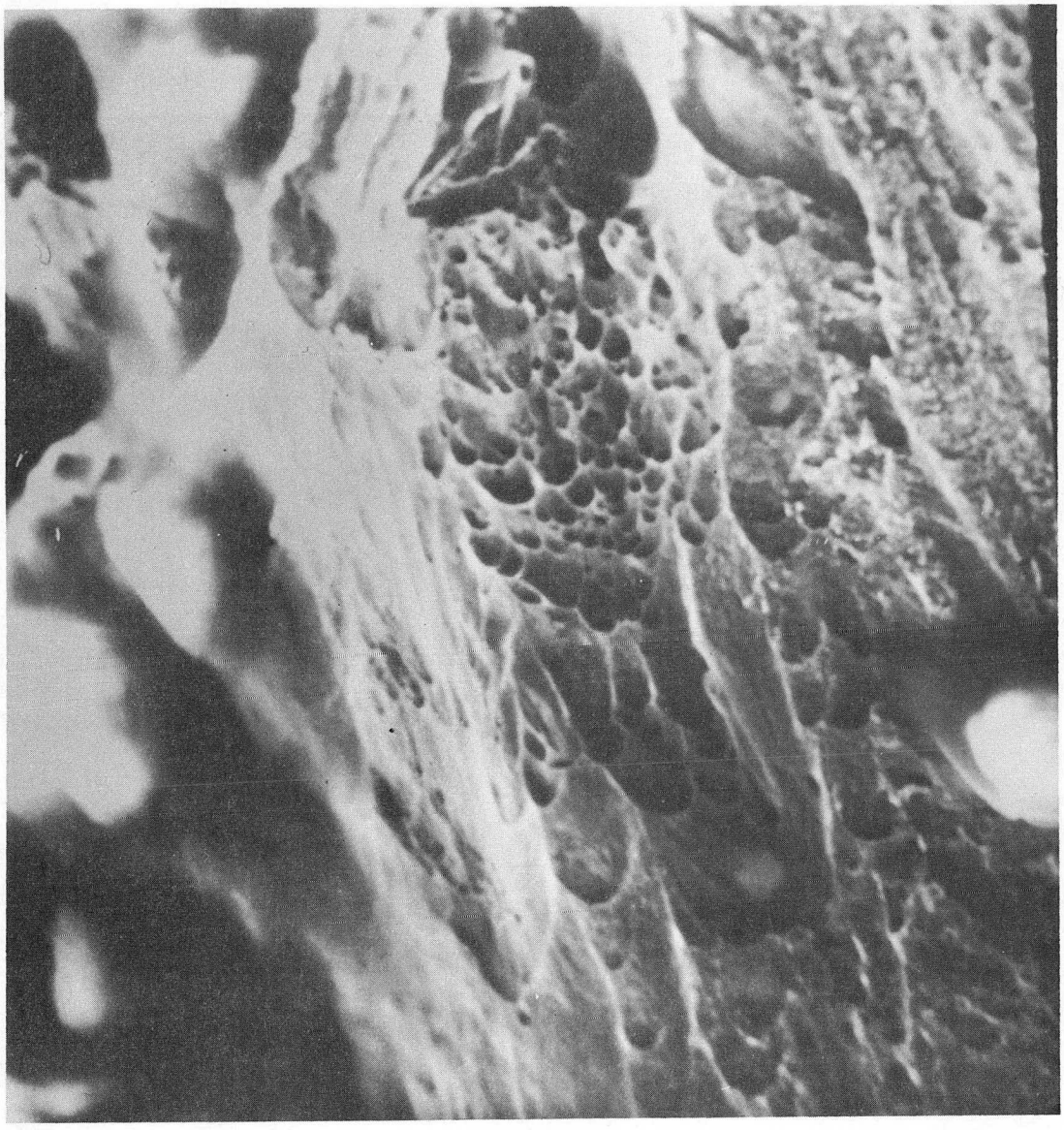

XBH671 19

Fig. 13

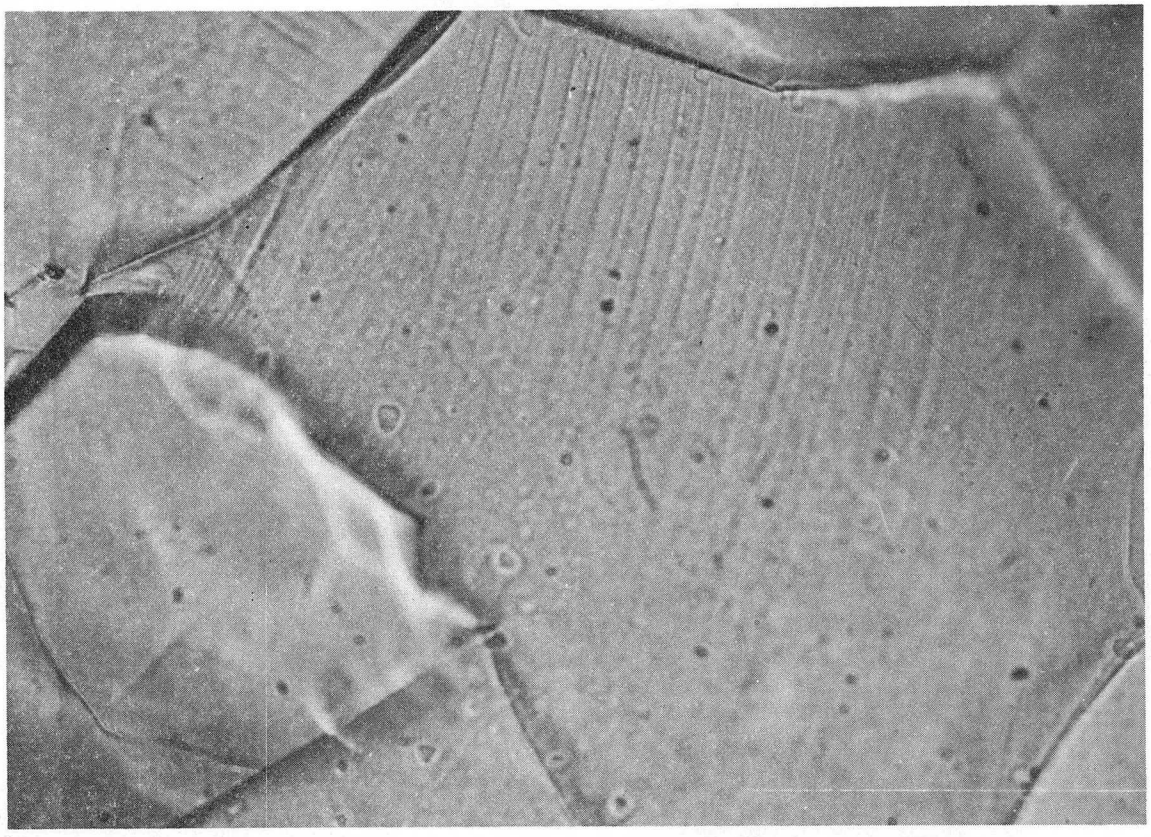

ZN-5797

Fig. 14

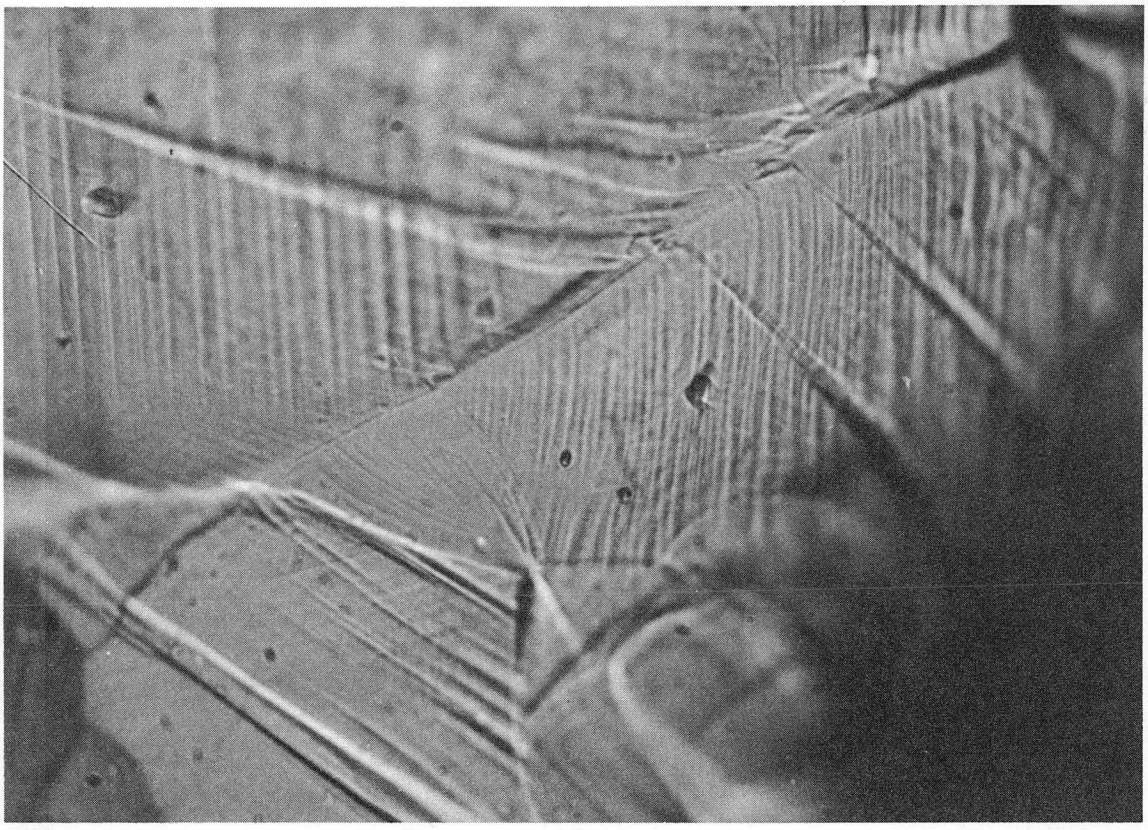

ZN-5800

Fig. 15

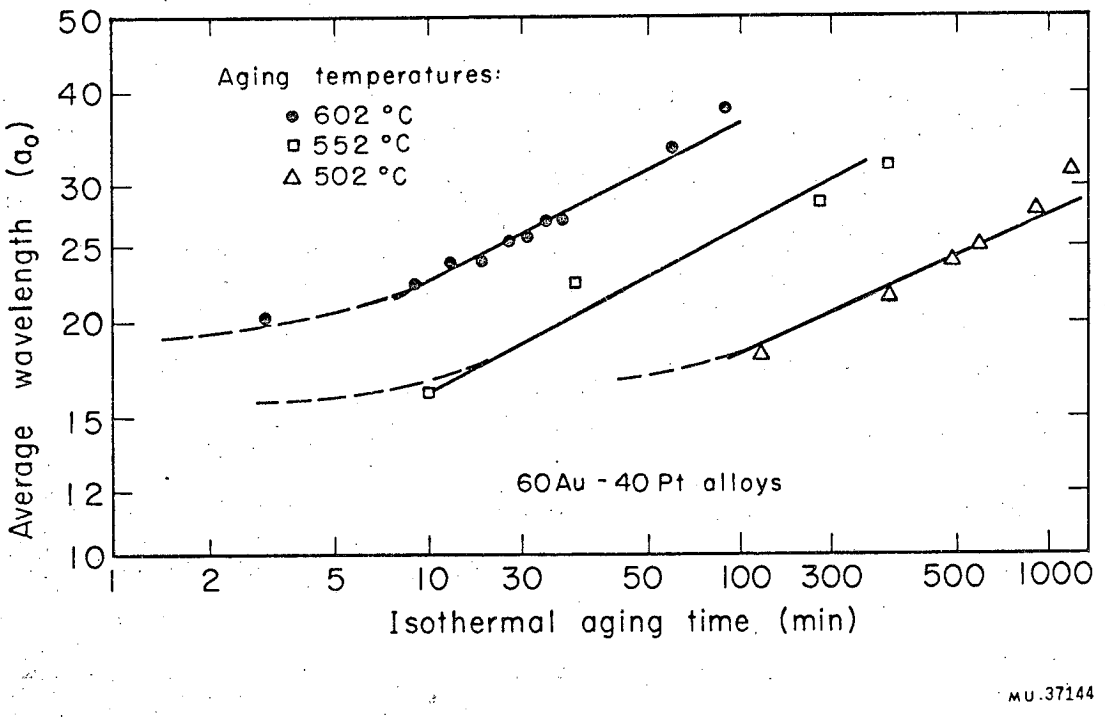
Aging temperatures:
602 °C
552 °C
502 °C
60Au - 40Pt alloys
Average wavelength (a_o)
Isothermal aging time (min)
50
40
30
25
20
15
12
10
1
2
5
10
30
50
100
300
500
1000
MU.37144

Fig. 16

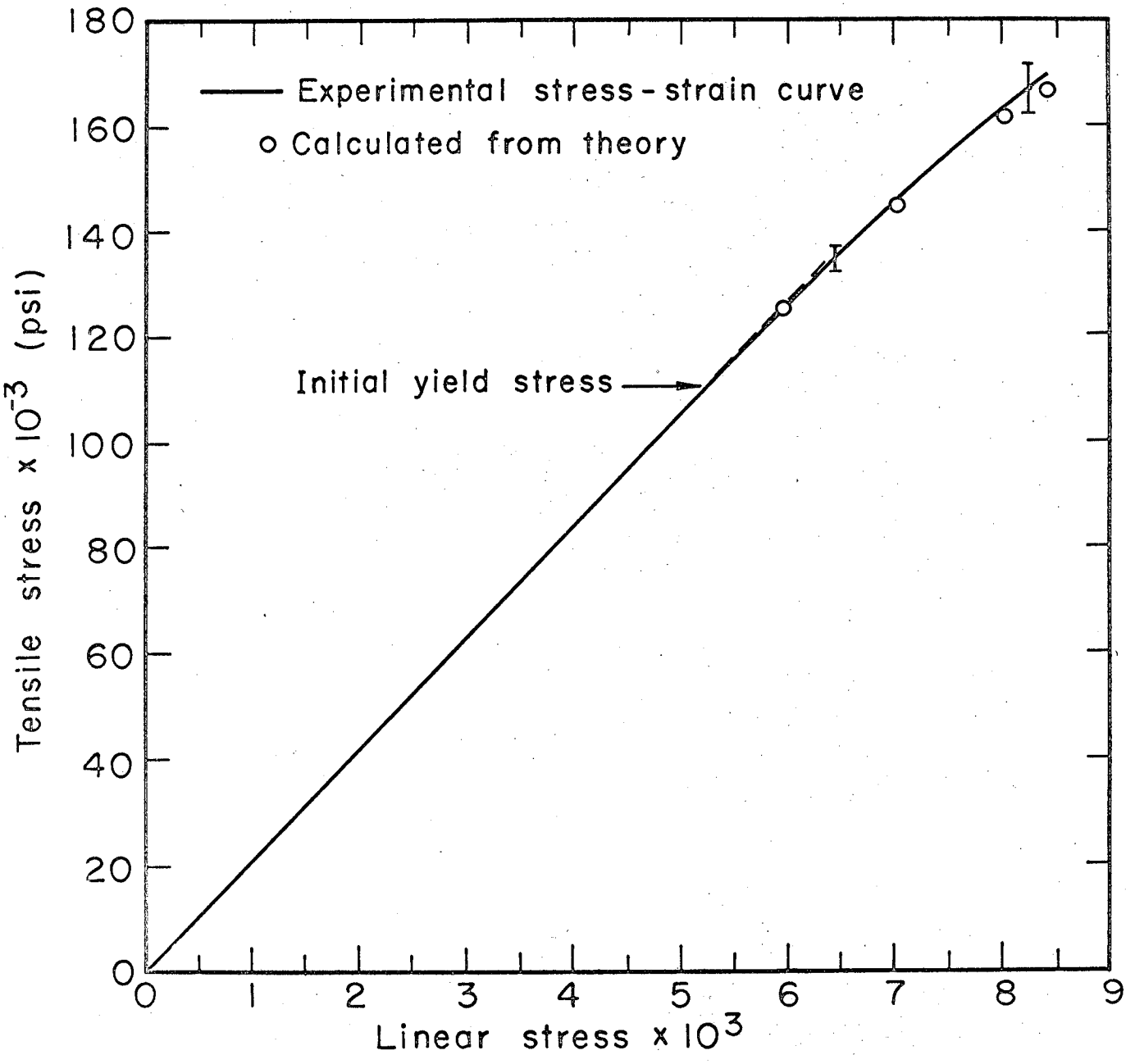
Experimental stress-strain curve
Calculated from theory
Initial yield stress
Tensile stress x 10^{-3} (psi)
Linear stress x 10^{3}
0
20
40
60
80
100
120
140
160
180
0
1
2
3
4
5
6
7
8
9
MU-37140

Fig. 17

This report was prepared as an account of Government sponsored work. Neither the United States, nor the Commission, nor any person acting on behalf of the Commission:

A. Makes any warranty or representation, expressed or implied, with respect to the accuracy, completeness, or usefulness of the information contained in this report, or that the use of any information, apparatus, method, or process disclosed in this report may not infringe privately owned rights; or

B. Assumes any liabilities with respect to the use of, or for damages resulting from the use of any information, apparatus, method, or process disclosed in this report.

As used in the above, "person acting on behalf of the Commission" includes any employee or contractor of the Commission, or employee of such contractor, to the extent that such employee or contractor of the Commission, or employee of such contractor prepares, disseminates, or provides access to, any information pursuant to his employment or contract with the Commission, or his employment with such contractor.